Metal-layer-assisted coalescence of Au nanoparticles and its effect on diameter control in vapor-liquid-solid growth of oxide nanowires

Dong Lai Guo,[1] Xiao Huang,[2] Guo Zhong Xing,[1] Zhou Zhang,[1] Gong Ping Li,[1] Mi He,[1] Hua Zhang,[2] Hongyu Chen,[1] and Tom Wu[1,*]

[1]*School of Physical and Mathematical Sciences, Nanyang Technological University, Singapore 637371, Singapore*
[2]*School of Materials Science and Engineering, Nanyang Technological University, Singapore 637371, Singapore*

(Received 30 August 2010; revised manuscript received 15 November 2010; published 4 January 2011)

By using the Au-catalyzed vapor-liquid-solid growth of ZnO and In_2O_3 nanowires as examples, we demonstrate the critical role of the coalescence of Au catalyst nanoparticles in determining the final diameter distribution of oxide nanowires. The enhanced coalescence is facilitated by a transient liquid-state metal layer in the initial nucleation stage. The onset and the thickness of this layer are dictated by the metal-vapor pressure and the distance between Au catalyst nanoparticles. Equipped with this insight, we are able to control the diameter of the oxide nanowires by tuning the thickness of the liquid-metal layer and the coalescence of the Au nanoparticles.

DOI: 10.1103/PhysRevB.83.045403 PACS number(s): 68.37.−d, 81.07.−b

I. INTRODUCTION

The vapor-liquid-solid (VLS) method has attracted much attention owing to its ability to produce a wide range of high-quality nanowires (NWs) to sustain the relentless developments in nanosciences and nanotechnologies.[1,2] It was first proposed more than four decades ago to explain the growth behaviors of Si whiskers.[3,4] In the conventional VLS growth of NWs composed of elemental materials such as Si and Ge [see the schematic in Fig. 1(a)], the liquid-state catalyst nanoparticles (NPs) absorb the material supplied from a vapor source and form alloy NPs, then the heterogeneous precipitation at the NP-substrate interface and the axial NW growth begin when supersaturation is reached in the alloy NPs.[1–4] Although this ideal model ignores the rich kinetics of liquid-catalyst droplets during the axial growth of NWs, such as the surface migration of the catalyst[5] and the interaction between the catalyst and the sidewall of the NW,[6] it points out the key role of the catalyst NP size in determining the diameter of the grown NWs. This size correlation between the catalyst NPs and the grown NWs was directly observed by Wu and Yang by using a transmission electron microscope (TEM),[7] and is often taken as a norm in NW synthesis. This precise diameter control is critical because the diameter of the NWs often determines their properties, such as the electronic band structure and the surface-to-volume ratio,[8–10] which in turn enables their applications in devices including photovoltaic cells,[11,12] sensors,[13,14] transistors,[15–18] and so on. Until now, the conventional VLS mechanism could describe satisfactorily the NW growth involving binary systems, e.g., Au-Si and Au-Ge, but some fundamental questions still remain regarding the nonequilibrium state and the dynamic behavior of catalyst NPs in the growth of multielement compounds, in particular, metal oxides.

It is of vital importance to address these fundamental questions considering the increasing interest focused on NWs of metal oxides, such as ZnO and In_2O_3, owing to their promising properties.[11,14,19–21] In the VLS growth of metal-oxide NWs, both the metal and the oxygen play important roles, which induce many more complexities. For example, the growth of ZnO NWs cannot be fully elucidated by the pseudobinary-phase diagram of Au-ZnO because the growth often occurs in the Zn-rich environment.[22] Unfortunately, an Au-Zn-O ternary-phase diagram does not exist in literature, which is also the case for many other oxides. Furthermore, the mutual interactions between the metal, oxygen, and the catalyst are highly susceptible to subtle changes in the growth environment, which stifles the in-depth understanding of the NW growth, and it remains a pressing issue to understand the dynamics of Au NPs during the initial growth stage. Furthermore, in routine oxide NW synthesis, continuous thin films are often found underneath the NWs, which are usually attributed to the competition between the conventional thin-film growth and the NW growth, but it is often unclear how this affects the NW morphology. As applications of oxide NWs are becoming more intensive, it is imperative to address these open issues in order to find universal strategies to achieve effective and reliable controls on the growth of oxide NWs.

Herein, we demonstrate that in the Au-catalyzed VLS growth of metal-oxide NWs, particularly in the initial nucleation stage, the role of a liquid-state metal layer is of critical significance. The formation of the metal layer is collectively determined by the metal-vapor pressure and the distance between Au NPs. Once such a transient liquid-state layer forms, it intimately interacts with the catalyst NPs before the heterogeneous precipitation and the NW growth. We use the VLS growth of ZnO and In_2O_3 NWs as examples to determine the experimental conditions for this liquid-metal layer to appear, and to illustrate its role in assisting the migration and coalescence of Au NPs, which eventually determines their size as well as the NW diameter [see Fig. 1(b)]. Equipped with this insight, we effectively tune the diameters of ZnO and In_2O_3 NWs by controlling the coalescence of Au NPs.

II. EXPERIMENT DETAILS

The experimental setup for the vapor transport growth of oxide NWs consisted of a horizontal tube furnace (Lindberg/Blue Mini) equipped with a gas supply and pumping systems. In order to grow ZnO NWs on *a*-plane sapphire substrates, ZnO and graphite powder (total weight: 8–32 mg; 5:1 weight ratio) was mixed by grinding for 30 min and then used as the source. The *a*-plane sapphire substrates (5×5 mm^2) were cleaned by

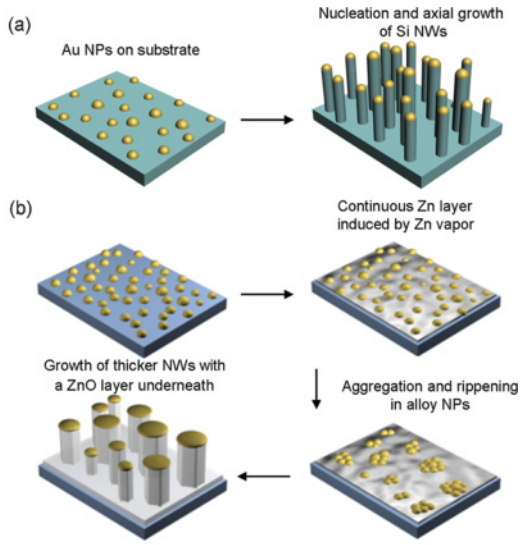

FIG. 1. (Color online) Conventional VLS growth mechanism of (a) elemental NWs (e.g., Si NWs) and (b) the proposed metal-layer-assisted growth of ZnO NWs.

ultrasound in acetone and annealed in air at 1000°C to achieve an atomically flat surface. Then an Au catalyst layer with a calibrated thickness (1–6 nm) was deposited by sputtering. The substrates were placed 3.5 cm downstream from the source in the furnace. During the growth, Ar mixed with O_2 (0.5%) was used as the carrying gas with a constant flow rate of 50 standard cubic centimeters per minute (SCCM). The pressure in the furnace tube was kept at 24 mbar. The temperature was ramped up at a rate of 50°C/min. The furnace was turned off immediately when its temperature reached 950°C and cooled down to room temperature.

The configuration of the experimental setup to grow In_2O_3 NWs on Si (100) substrates is similar. In a typical experiment, In_2O_3 and graphite mixed powder (1:1 weight ratio) was used as the source, which was placed at the center of the furnace. Si (100) substrates coated with a 3-nm Au layer were placed 3 cm downstream. Ar mixed with 0.05% O_2 was used as the carrying gas. Its flow rate and the pressure inside the furnace tube were kept at 50 SCCM and 15 mbar, respectively. During growth, the furnace temperature was ramped at a rate of 50°C/min to 950°C, held for 30 min, and then cooled down to room temperature.

The composition and the crystalline structure of the grown samples were determined by x-ray diffraction (XRD). A JEOL JSM-6700 F field-emission scanning electron microscope (SEM) was used to study the sample morphology. Transmission electron microscopy (TEM) and scanning transmission electron microscopy (STEM) images were obtained on a JEOL JEM-2010 TEM. The composition measurements were performed by an energy-dispersive x-ray spectrometer (EDS) attached to the TEM.

III. RESULTS AND DISCUSSION

A. Coalescence of Au catalyst NPs and their effect on ZnO NW growth

It is well known that metal nanostructures exhibit size-dependent melting behaviors, and thin metal layers often melt at temperatures much lower than the bulk melting point. NPs form as a result of dewetting on the supporting substrates owing to the Rayleigh instability and the weak interfacial metal-substrate interaction.[23,24] The density and size of metal NPs depend on the thickness of the metal layer and the annealing conditions. To prepare Au catalyst NPs with controlled density, we systematically tuned the thickness of sputtered Au thin layers. In our experiment, the thickness of the Au catalyst layers was tuned from 1 to 6 nm. Six corresponding ZnO NW samples labeled Z16-1 to Z16-6 were fabricated by using the same source weight of 16 mg. To obtain the statistics of the NW-NP diameter, for each sample more than 300 NWs-NPs were surveyed, and their average value and standard deviation were calculated.

As a result of minimization of the total surface free energy, growth of larger Au NPs is known to occur at high temperatures, which significantly affects the diameter distribution of the Au NPs.[5,25,26] To simplify the sintering environment, primary Au NPs were prepared in the control experiments without the ZnO-graphite source powder while all the other experimental conditions were kept the same. The furnace temperature was ramped to 950°C and then cooled down immediately. SEM images of the Au NPs after the thermal cycles are shown in the insets of Figs. 2(a)–2(f). As expected, the thin Au layers dewet the sapphire substrates

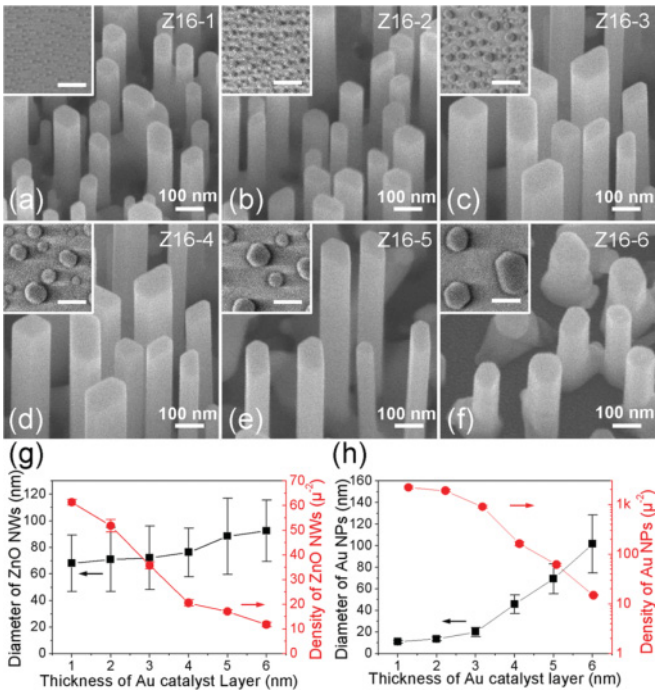

FIG. 2. (Color online) (a)–(f) SEM images of ZnO NWs grown on sapphire substrates by using 1–6 nm Au layers as a catalyst. The source weight is fixed at 16 mg. The tilting angle during the SEM observation is 20°. The labels of the samples are shown on the right-hand top corners of the images. The same source weight of 16 mg was used for all six samples. Insets: SEM top views of the Au NPs after the Au layers were heated without the source powder and the ZnO NW growth. All scale bars: 100 nm. (g) Plot of diameter and density of the ZnO NWs vs thickness of the Au layers. (h) Plot of diameter and density of the Au NPs vs thickness of the Au layers.

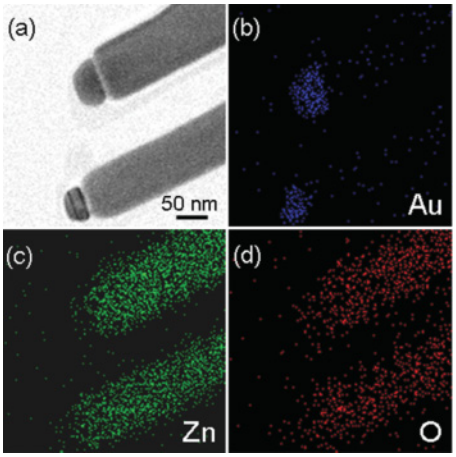

FIG. 3. (Color online) (a) STEM image of ZnO NWs in sample Z16-1 with Au NPs on the NW tips, suggesting a VLS-dominant growth mechanism. (b)–(d) EDS element mappings of Au, Zn, and O, respectively.

at the high temperature and Au NPs are formed on the substrate surface. As the thickness of the Au layer changes from 1 to 6 nm, the average density of the Au NPs decreases from 2222 ± 72 to 15 ± 1 μm^{-2}. Concurrently, the average size of the Au NPs significantly increases from 11 ± 1.3 to 100 ± 27 nm. This increase of the diameter of Au NPs is collectively determined by the Rayleigh instability and the thickness inhomogeneity of the Au layer.[24]

Does the growth of ZnO NWs shown here follow the VLS mechanism? It has been demonstrated recently that the catalyst is not the prerequisite for the NW growth; surface roughness and structural dislocations could provide energetically favored nucleation sites and initiate the growth of NW.[27,28] To answer this question on growth mechanism, we examined in detail the structure of the NWs by using electron microscopes. The ZnO NW tips show no clear contour of Au NPs in the top-view SEM images [Figs. 2(a)–2(f)]. However, further STEM and EDS mappings of the NWs (Fig. 3) clearly reveal that Au-rich NPs with facetted surfaces are visible on the NW tips and certify that the growth of ZnO NWs is dominated by the Au-catalyzed VLS growth mechanism. During the VLS growth, these Au NPs are presumably in the liquid state, and their dome shape is determined by the balance of the surface tension and the interface energies. Although this observation of Au NPs on the NW tips does not completely exclude the possibility of self-catalyzed growth in some NWs,[29] it suggests strongly that VLS is the dominating growth mechanism and validates our following analysis.

Similar to the findings of previous reports,[20,30] the density of ZnO NWs decreases from 61 ± 2 to 12 ± 1 μm^{-2} as the Au layer becomes thicker. What attracted our attention is that the average diameter of ZnO NWs increases only modestly, i.e., from 68 ± 15 to 93 ± 16 nm, although the average size of the Au NPs increases from 11 ± 1.3 to 100 ± 27 nm. This strong discrepancy between the diameter distribution of ZnO NWs and that of Au NPs is often overlooked in routine NW growth, which, however, warrants in-depth investigations. The dependence of the diameter and the density of the as-grown ZnO NWs and Au NPs on the initial thickness of Au catalyst layers is plotted in Figs. 2(g) and 2(h), respectively. The trend is quite clear: When the Au layer is thicker, the dimension and density of ZnO NWs follow those of Au NPs very well; on the other hand, the deviation between them becomes significant when the Au layer is thinner.

To illustrate this discrepancy, we plot in Fig. 4(a) the ratios between the size of ZnO NWs and that of Au NPs as a function of the thickness of Au layers. The ratio reaches 6 when the thickness of the Au layer is 1 nm. This notable size mismatch between original NPs and NWs cannot be explained by the conventional VLS growth mechanism, where the condensation from the supersaturated NPs always suggests identical or similar dimensions. Our results shown in Fig. 2 suggest that the Au NPs can be as small as 11 nm, which is presumably still above the thermodynamic minimum radius of liquid-state metal NPs,[31] but the ZnO NWs are much thicker. On the basis of this reasoning, we hypothesize that sintering of the Au NPs is probably different with and without the presence of Zn vapor. Hence, two factors contribute to the size discrepancy between the Au catalyst NPs and the ZnO NWs: One is the size increase during the Au-Zn alloying process,[32] and the other is the coalescence of the catalyst NPs during the growth stage. To study these two effects independently, we carried out a series of control experiments by using prefabricated colloidal Au NPs with very low dispersion densities (less than 1 μm^{-2}, much smaller than $\sim$2000 μm^{-2} in Z16-1 formed from a 1-nm Au layer) to avoid the coalescence of NPs. Prefabricated colloidal Au NPs with diameters of 5, 15, 25, 40, 60, and 90 nm were used to grow ZnO NWs on sapphire substrates. The statistical result in Fig. 4(c) shows that the size of ZnO NWs catalyzed

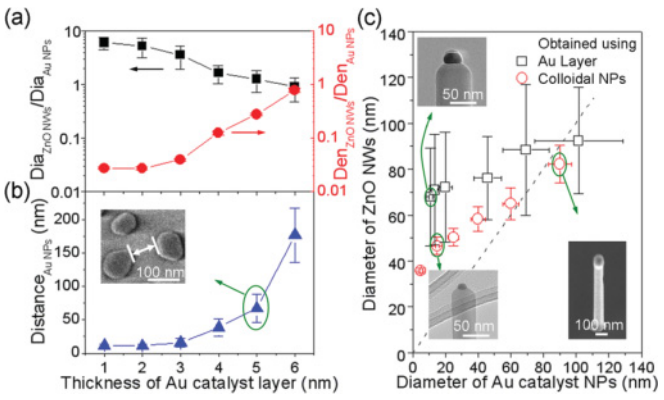

FIG. 4. (Color online) Effect of the thickness of Au layers on the ratios of diameter and density between ZnO NWs and Au NPs (a) and on the average border distance between Au NPs (b). Inset in (b): Border distance between Au NPs is illustrated in the SEM image of Au NPs formed from the 5-nm Au layer. (c) Effect of diameter of Au catalyst NPs on the diameter of grown ZnO NWs for both cases of thin films and colloidal NPs. The dashed line in the figure has a slope of 1. Top left inset: TEM image of a ZnO NW whose growth was catalyzed by the 1-nm Au layer, where the average size of the Au catalyst NPs is 11 nm while the ZnO NW diameter is 68 nm. Bottom left inset: TEM image of a ZnO NW catalyzed by colloidal Au NPs with a diameter of 15 nm. Bottom right inset: SEM image of a ZnO NW catalyzed by 90-nm colloidal Au NPs, and in this case the dimensions of Au NP and ZnO NW are almost identical. The tilting angle during the SEM observation is 20°.

by the colloidal Au NPs does not strictly follow that of the colloidal Au NPs (deviating from the dashed line in the figure) even though the coalescence of NPs does not play a role here. Similar to the case of growth catalyzed by Au layers, this size discrepancy is largest when the NPs are small; the NW diameter is ∼36 nm when 5-nm colloidal NPs were used. This compromised control on the NWs diameter can be attributed to the Zn absorption and the formation of Au-Zn alloy droplets at the thermodynamic equilibrium, which enlarges the original NPs and leads to thicker NWs.

However, the comparative data shown in Fig. 4(c) suggests that this alloying process alone cannot fully account for the poor NW diameter control when thinner Au layers were used as a catalyst. On the other hand, this supports the scenario that during the nucleation stage, after the dewetting of the Au thin layers, substantial coalescence between the Au NPs occurred under the presence of Zn vapor,[33] which modified the size distribution of Au NPs before the NW growth. The large NP sizes seen in Fig. 3(a) and the top left inset in Fig. 4(c) further support this scenario. The coalescence appears to depend on the thickness of the Au layer or equivalently on the distance between Au NPs. Figure 4(b) presents the modulation effect of the Au layer thickness on the average border distance between Au NPs. When the thickness of the Au layer is less than 3 nm, the distance between Au NPs is smaller than 25 nm. To minimize the total surface energy, small Au NPs incline to aggregate and form larger particles via the coalescence, leading to the growth of ZnO NWs (i.e., NWs in Z16-1) with diameters larger than those of the original Au NPs. The average distance between two neighboring NPs increases quickly when the Au layer is thicker. In particular, the distance between Au NPs approaches ∼175 nm at the 6-nm-thick Au layer, leading to much less coalescent events in Z16-6, and the size and density of ZnO NWs start to resemble those of Au NPs.

To understand this coalescence between Au NPs in the presence of Zn vapor, we have to consider the high-temperature alloying process between Au NPs and the Zn vapor. According to the Au-Zn binary-phase diagram, at a growth temperature of 900°C, Zn in the Au-rich solution saturates at ∼4%.[34] Hence, it is unlikely that the increase in the size of alloy droplets can solely account for the increase in the diameter of the resulting ZnO NWs. After the supersaturation is reached, Zn probably condenses out of the Au-Zn alloy NPs to form droplets. The size of the droplets is mainly determined by the global Zn vapor pressure in the furnace tube. To minimize the interface energy, the alloy NPs tend to stay on the surface of these liquid-state Zn droplets.[35] If a very thin layer of Au is used, as in the case of Z16-1, the resulting density of Zn droplets is very high, presumably as high as that of Au NPs as shown in the inset of Fig. 2(a). Because the initial distance between Au NPs is short [e.g., ∼12 nm when the thickness of the Au layer is 1 nm, as shown in Fig. 4(b)], these Zn droplets may make contact with each other and then merge into a continuous liquid-state network. Because the active Zn shows a large enthalpy of formation of oxide, the interfacial interaction between the Zn and oxide substrate is strong and thus the continuous liquid layer exhibits good wettability.[24] This stable layer provides migration paths for the coalescence of Au NPs. In other words, the formation of a continuous metallic Zn layer occurs during the coalescence of Au NPs and facilitates the latter. As a result, larger Au NPs with a lower density are formed, which eventually leads to the growth of thicker ZnO NWs. On the other hand, when the original Au layer is thick, e.g., 6 nm as in sample Z16-6, the Zn droplets are less likely to merge with each other to form a continuous layer owing to the fact that the distances between Au NPs are larger. No continuous Zn layer is formed and Zn droplets remain separated throughout the whole process, leading to similar dimensions between ZnO NWs and Au NPs. Therefore, whether a liquid-state Zn layer exists determines the characteristics of the coalescent process and the size distribution of the grown ZnO NWs.

During the growth process, this transient liquid-metal layer gradually solidifies into a continuous ZnO layer, which terminates the migration and coalescence of catalyst NPs. Naturally this ZnO layer emerging from the oxidized Zn layer may also assist in the epitaxial growth of aligned ZnO NWs on top. Extensive SEM studies revealed a close correlation between the Au NP coalescence and the formation of a ZnO buffer layer underneath the NWs after the VLS growth. A typical example is shown for sample Z16-1, where the vertical ZnO NWs do not stand directly on the substrate [see Fig. 2(a)], but on a continuous buffer layer. Such a buffer layer underneath the NWs has been reported previously, however, its role in the NW growth has not been elucidated so far. In contrast to Z16-1, no such buffer layer existed in sample Z16-6 where the coalescent events were inhibited, and all NWs grew directly on the sapphire substrate [see Fig. 2(f)].

B. Effect of metal-vapor pressure on the formation of a transient metal layer and the diameter control

Because the formation of a continuous layer underneath the ZnO NWs is critically important for diameter distribution, what are the factors determining its onset and characteristics? In our system, in order to form a continuous transient metal layer, the liquid Au-Zn droplets must contact each other, which depends on the inter-NP distance and the size of Zn droplets. Regarding the first factor, we have discussed above in detail the experiments performed with different Au layer thicknesses. We now focus on the effect of Zn pressure and demonstrate that it is also a critical parameter.

Because the volume of the quartz tube is fixed (1 in. diam and 20 in. long), the Zn vapor pressure is presumably proportional to the source weight although its absolute value was not calibrated. The source powder with weights of 8, 16, 24, and 32 mg was used to generate different Zn vapor pressures while the thickness of the Au catalyst layers is fixed at 1 nm. The four grown samples are labeled Z8-1, Z16-1, Z24-1, and Z32-1, respectively. Their SEM images and the corresponding diameter distributions of NWs are shown in Fig. 5. Interestingly, consistent evolutions in the thickness of the buffer layers and the size distribution of ZnO NWs were observed. In sample Z8-1, where only 8 mg of source was used, no oxide buffer layer was observed and the diameter of the NWs is 42 ± 6 nm [see the inset of Fig. 5(a)]. In contrast, when four times more source was used to grow sample Z32-1, a thick buffer layer of ∼430 nm exists under the NWs and the diameter of the NWs increases to 110 ± 25 nm. These experimental observations support the theory that a higher Zn vapor induces

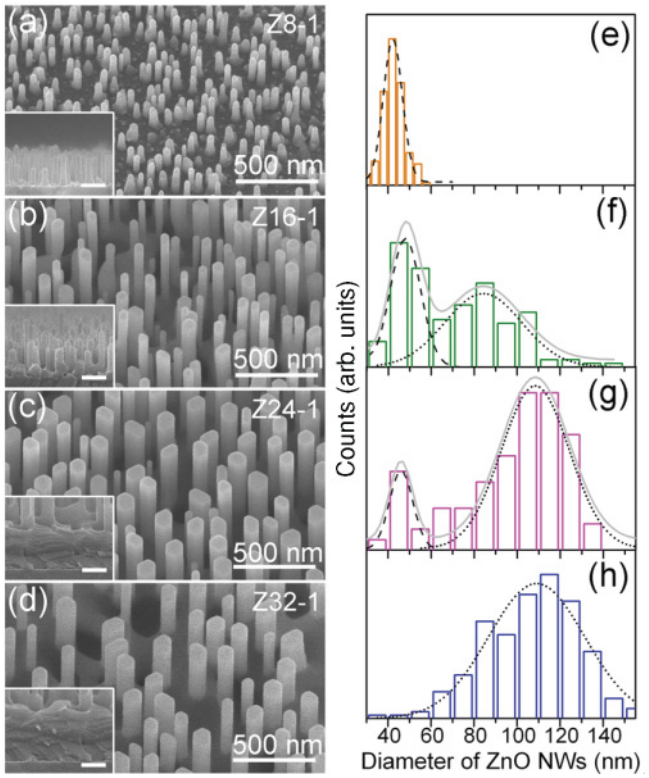

FIG. 5. (Color online) (a)–(d) SEM images of ZnO NWs grown by adjusting the Zn vapor pressure while the Au layer thickness was fixed at 1 nm. The tilt angle during the SEM observation is 20°. The source weights were rationed as (a) 8, (b) 16, (c) 24, and (d) 32 mg, respectively. Insets: Corresponding cross-sectional SEM images showing the ZnO buffer layers with different thickness. All scale bars in insets: 200 nm. (e)–(h) Histograms showing the distributions of NW diameters corresponding to panels (a)–(d), respectively.

larger Zn droplets and facilitates the formation of a continuous metal layer, which assists the coalescence among Au NPs and the growth of thicker ZnO NWs. Furthermore, bimodal distributions of the NW diameters were observed [see Figs. 5(f) and 5(g)] in samples with intermediate source weights, i.e., Z16-1 and Z24-1. As the Zn vapor pressure increases, the peak at 42 nm continuously decreases, while another peak appears at larger diameters, which arises from the stronger coalescence assisted by the thicker liquid layers. Thus, with the assistance of a liquid Zn layer, merging among Au NPs gradually reduces the population of the original Au NPs ($\sim$2000 μm^{-2}) and leads to the formation of larger Au NPs. Similar bimodal distributions and size evolution were also observed in the aggregation of silver-coated Au NP colloids,[36] and an inverse process was reported in the process of deagglomeration of silica NPs in surfactants.[37]

C. Liquid-state Zn layer as a buffer layer assisting the coalescence of Au NPs and the ZnO NW growth

Figure 6 summarizes the effects of the inter-NP distance and the metal-vapor pressure in the formation of the transient metal layer and the ZnO NW growth. When the Au layer is thick, e.g., 6 nm, the size and density of the ZnO NWs resemble the size and density of the Au NPs [Figs. 6(a) and 6(d)]. However, when the thickness of the Au layer decreased, both the size and density of the grown ZnO NWs do not follow those of the catalyst Au NPs owing to the enhanced coalescence between the Au NPs [Figs. 6(b) and 6(e)]. A signature of this process is the observation of a continuous ZnO layer between the ZnO NWs and the sapphire substrate. The formation of this ZnO layer also depends on the Zn vapor pressure, which facilitates the coalescence of Au NPs. When less source powder was used, the formation of the liquid Zn layer is

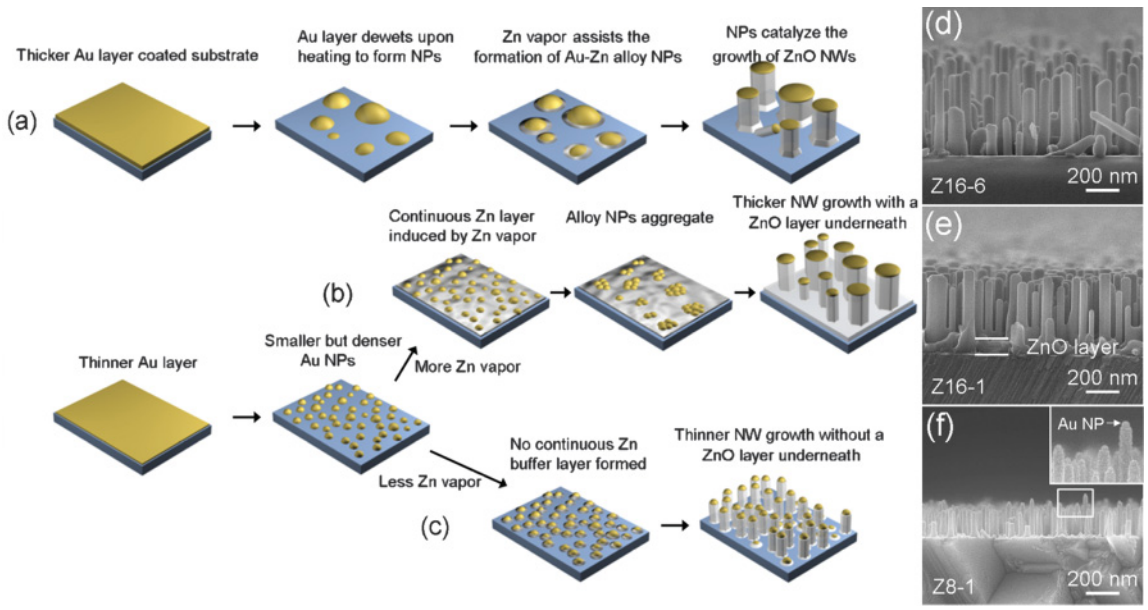

FIG. 6. (Color online) (a)–(c) Schematics illustrating the critical roles of the thickness of Au catalyst layers and the vapor pressure of Zn in affecting the VLS growth of ZnO NWs by controlling the onset of transient Zn-metal layers and the subsequent coalescent events between the Au catalyst NPs. (d)–(f) Cross-sectional SEM images of the ZnO NWs grown on sapphire substrates corresponding to (a)–(c), respectively. Experimental parameters: (a) and (d) Au catalyst layer, 6 nm and source, 16 mg; (b) and (e) Au catalyst layer, 1 nm and source, 16 mg; (c) and (f) Au catalyst layer, 1 nm and source, 8 mg. Inset in (f): Magnified image of the selected area.

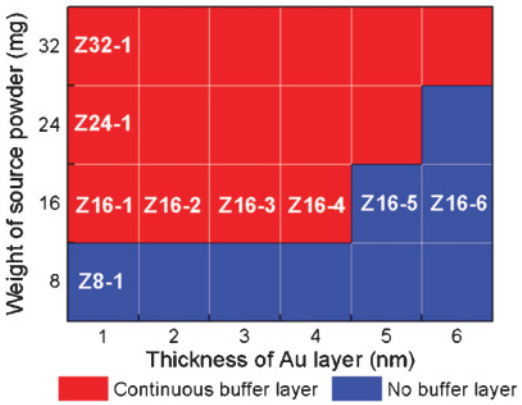

FIG. 7. (Color online) Effect of the thickness of the Au layer and source weight on the formation of oxide buffer layers.

suppressed, which enables the growth of thinner ZnO NWs [Figs. 6(c) and 6(f)]. Figure 7 gives a complete diagram summarizing the experimental results of 24 runs of growth of ZnO NWs. The thickness of the Au catalyst layer and the source weight determine the distance between the Au NPs and the Zn vapor pressure, respectively, which collectively dictate the onset and the characteristics of the metal layer.

To achieve a deeper understanding of this solid-state ZnO layer, we investigated its structure in detail by using high-resolution TEM (HRTEM) and selected-area electron diffraction (SAED). As shown in Fig. 8(a), it appears to be a single-crystal ZnO epitaxially formed on the *a*-plane sapphire, which is not surprising considering the good lattice match and the preferred growth of ZnO along the *c* direction.[30] The observed lattice deformation in ZnO near the interface [Fig. 8(b)] may originate from the lattice mismatch and the growth-related strain. The HRTEM image taken near the ZnO-sapphire interface [Fig. 8(c)] suggests that all of the ZnO NWs are coherently grown on the ZnO layer without any visible interface or transition region. These TEM results confirm that the transient Zn layer is fully converted to the ZnO phase, and the epitaxial growth of ZnO NWs is preserved during the synthesis.

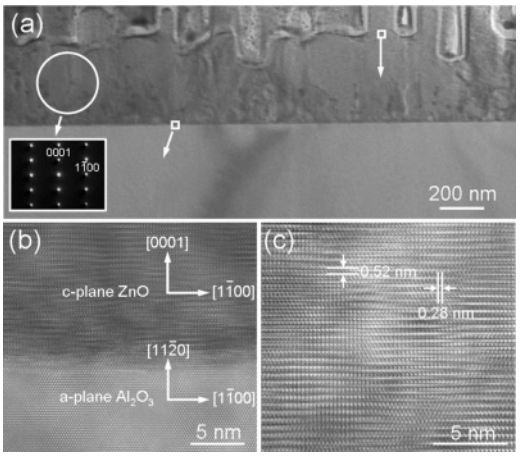

FIG. 8. (a) Cross-sectional TEM image of ZnO NW sample Z32-1 taken along the ZnO[$\bar{1}\bar{1}$20] zone axis. The ZnO-sapphire interface can be clearly observed. Inset: SAED pattern corresponding to the selected area in (a). (b), (c) HRTEM images corresponding to the selected areas in (a).

This NW diameter modulation by the transient liquid-metal layer is different from the previously reported strategies of template-directed nucleation control.[38] Instead, the metal-layer-assisted coalescence of Au NPs proposed here is analogous to the buffer-layer-assisted growth (BLAG) reported previously.[39,40] In BLAG, a solid-state buffer layer is first grown on the substrate at a low temperature and then coated with a thin layer of metal. Once the substrate is heated, rapid desorption of the buffer layer induces metal NPs to migrate and coalesce. The size of the formed metal particles depends strongly on the thickness of the buffer layer because the thicker buffer layer provides a longer time for NPs to migrate and collide, resulting in larger NPs. In the conventional BLAG model, the evaporation of the buffer layer terminates the NP dynamics. Similarly, in our case, the oxidized liquid-metal layer becomes a single-crystal ZnO layer and fixes the alloy NPs in place, which is the critical stage dictating the size distribution of the grown NWs.

In a two-dimensional system, the number of binary collisions responsible for the particle coalescence is proportional to $\delta D(r)C^2$, where δ is the collision efficiency, $D(r)$ is the equivalent diffusion coefficient, and C is the particle concentration. In our case, δ should be equal to 1, since the van der Waals force between Au NPs is always attractive.[39] A thinner Au layer leads to a higher density of Au NPs, or a larger C, which implies more collisions between Au NPs and a stronger coalescence. This is consistent with the experimental results obtained by varying the thickness of the Au layer. Furthermore, if the thickness of the Au layer is fixed, a higher Zn vapor pressure leads to a thicker liquid Zn layer, which boosts the diffusion coefficient $D(r)$. Accordingly, more collisions and coalescences between Au NPs are expected, leading to the formation of larger Au NPs and then the growth of thicker ZnO NWs.

D. Effect of the transient metal-layer formation on the general VLS growth of oxide NWs

Now we discuss how general this model of metal-layer-assisted coalescence is in the context of oxide NW synthesis. The experiments delineated herein start with Au ultrathin films, which give Au NPs with a controlled size and density at high growth temperatures. Thus, it is straightforward for our results to be applied to the general scheme of using Au thin films to catalyze the growth of oxide NWs. It is also relevant to the experiments, where prefabricated Au colloidal NPs are directly used and dispersed on the growth substrates with high densities. Similarly, in such experiments, good control on the NW diameter can be realized only if the metal-layer-assisted coalescence is avoided, typically by using Au NPs of low densities. In general, coalescence of Au NPs has to be considered if the metal-vapor pressure is high enough and the distance between Au NPs is short enough, which are the prerequisites for the formation of a transient metal layer. Note that usually the dispersed colloidal NPs are not dense enough to induce strong coalescence, where a good size correspondence between the Au colloidal NPs and the grown NWs is often observed.

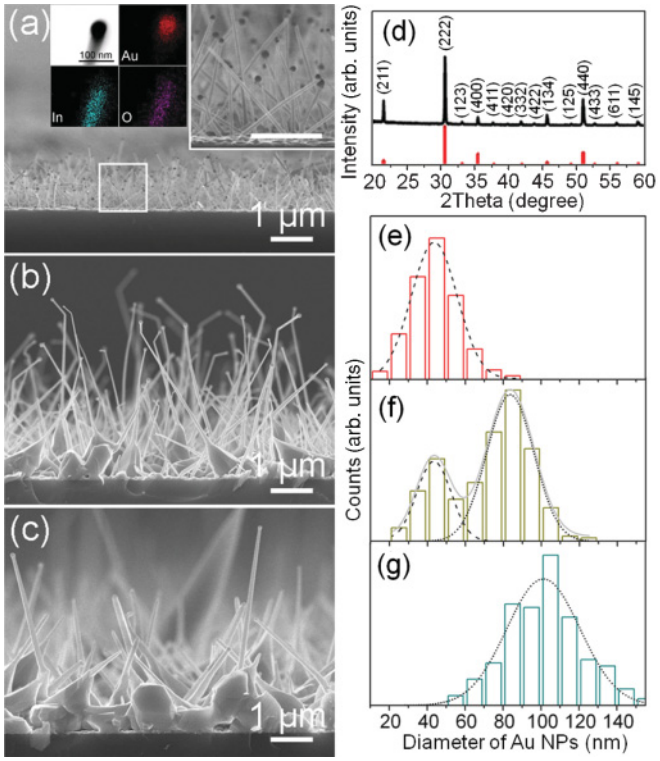

FIG. 9. (Color online) (a)–(c) Cross-sectional SEM images of In_2O_3 NWs grown with different In vapor pressures. The source weights were rationed as (a) 30, (b) 40, and (c) 50 mg, respectively. Top left inset in (a): STEM and EDS element mappings images of an In_2O_3 NW taken from sample IO30 with an Au NP on its tip, suggesting a VLS-dominated growth mechanism. Top right inset in (a): Magnified SEM image of the selected area. Scale bar: 500 nm. (d) XRD pattern of In_2O_3 nanowires. The reference powder diffraction data (JCPDS Card No. 89-4595) is also shown at the bottom. (e)–(g) Size distributions of Au NPs at the tips of In_2O_3 NWs shown in (a)–(c), respectively.

The metal-layer-assisted coalescence of Au NPs should be a universal phenomenon in the VLS growth of many other metal-oxide NWs, besides ZnO. To examine this hypothesis, we carried out experiments to grow In_2O_3 NWs on Si (100) substrates to investigate the possible coalescence of Au NPs assisted by a liquid In layer. The Au-Zn and the Au-In systems have similar binary-phase diagrams in the range of 800–1000°C.[34] A series of samples were grown by systematically varying the source weight while the In_2O_3-graphite ratio was fixed at 1:1. Samples IO30, IO40, and IO50 correspond to source weights of 30, 40, and 50 mg, respectively.

The cross-sectional views of these samples were shown in Figs. 9(a)–9(c). The XRD data of the as-grown In_2O_3 NWs shown in Fig. 9(d) is consistent with the bixbyite In_2O_3 structure (JCPDS Card No. 89-4595, $a = 1.011$ nm). Compared with the ZnO case, the Au NPs at the tips of the In_2O_3 NWs appear more spherical, indicating a larger wetting angle [see the inset of Fig. 9(a)]. The size distributions of Au NPs in IO30-50 are plotted in Figs. 9(e)–9(g). In IO30, uniform NWs were directly grown on the substrate without any buffer layer in between. The average size of the Au NPs

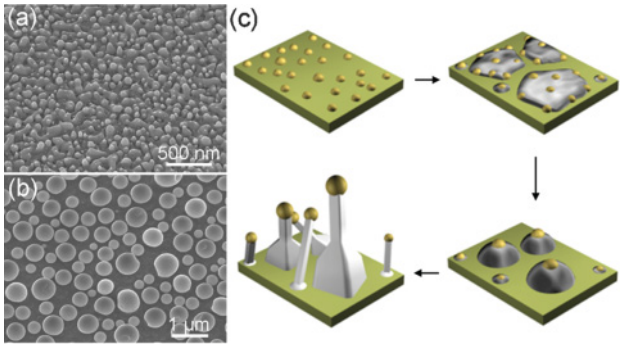

FIG. 10. (Color online) (a) Continuous Zn layer formed on the *a*-plane sapphire substrate when pure Ar was used as the carrying gas and a 1-nm Au layer was used as the catalyst, suggesting the good wetting of Zn with the substrate. (b) Separated In spheres formed on the Si (100) substrate when pure Ar was used as the carrying gas, which can be attributed to the poor wetting between In and the Si substrate. (c) Proposed metal-layer-assisted coalescence of Au NPs and its effect on the growth of In_2O_3 NWs.

at the tips of the NWs is 43 nm, which is slightly larger than that of the NWs (30 nm). A higher In vapor pressure exerts a large impact on the size distribution of the In_2O_3 NWs in sample IO40, where NWs can be divided roughly into two groups. The NWs in one group grow directly on the substrate with a uniform diameter similar to the NWs in sample IO30. The other group has larger Au NPs (80 nm in average) at their tips as well as big bases at the bottom. In sample IO50, a continuous buffer layer forms under the NW arrays, and the average size of the Au NPs increases to 100 nm. Unlike the case of Zn on sapphire, the liquid-state In does not wet the Si surface very well [see the comparison in Figs. 10(a) and 10(b)]. In a control experiment, we studied the wetting behaviors by using pure Ar as the carrying gas. Indeed, the continuous Zn layer was observed on sapphire owing to the good wetting. In contrast, separated In spheres with a wide distribution of size were formed on the Si substrate, indicating a poor wetting behavior. As a result, sample IO40 exhibits a discontinuous buffer layer, accompanied by small individual islands, which contributes to the bimodal size distribution in Fig. 9(f). Figure 10(c) illustrates the growth process. Substantial coalescence between the In islands only occurs at high In vapor pressures, e.g., in IO50, where a continuous buffer layer forms.

IV. CONCLUSIONS

In summary, we showed that the coalescence of Au NPs at the initial VLS growth stage of metal-oxide NWs must be considered carefully in order to achieve high-quality reproducible NW growth with tunable size distribution. The main thread of our work is to identify the metal layer as the key factor dictating the coalescence of Au NPs by adjusting the initial NP density and manipulating the thermodynamic parameters involved in the process. We used ZnO and In_2O_3 NWs as examples to quantitatively reveal the mechanism by systematically collecting statistic data. Tuning the metal-vapor pressure was found to be an effective way to adjust the thickness of the liquid-metal layer, and to achieve controls on

the size distribution of the catalyst NPs as well as the grown NWs. Good correspondence between catalyst NPs and oxide NWs can be achieved only when the onset of the oxide buffer layer and the coalescence of NPs are avoided. The oxide buffer layers with controlled thicknesses may also exert influence on the various physical and chemical properties of the oxide NWs, which is beyond the scope of this paper. In general, we believe the proposed metal-layer-assisted coalescence mechanism has implications on the synthesis of a wide range of metal-oxide NWs, complementing the conventional VLS scenario.

ACKNOWLEDGMENT

This work was supported by the Singapore National Research Foundation (RCA-08/018).

*tomwu@ntu.edu.sg

[1] A. M. Morales and C. M. Lieber, Science **279**, 208 (1998).
[2] S. Kodambaka, J. Tersoff, M. C. Reuter, and F. M. Ross, Phys. Rev. Lett. **96**, 096105 (2006).
[3] R. S. Wagner and W. C. Ellis, Appl. Phys. Lett. **4**, 89 (1964).
[4] E. I. Givargizov, J. Cryst. Growth **31**, 20 (1975).
[5] J. B. Hannon, S. Kodambaka, F. M. Ross, and R. M. Tromp, Nature (London) **440**, 69 (2006).
[6] T. Xu, J. P. Nys, A. Addad, O. I. Lebedev, A. Urbieta, B. Salhi, M. Berthe, B. Grandidier, and D. Stievenard, Phys. Rev. B **81**, 115403 (2010).
[7] Y. Y. Wu and P. D. Yang, J. Am. Chem. Soc. **123**, 3165 (2001).
[8] B. Delley and E. F. Steigmeier, Appl. Phys. Lett. **67**, 2370 (1995).
[9] J. E. Yang, C. B. Jin, C. J. Kim, and M. H. Jo, Nano Lett. **6**, 2679 (2006).
[10] K. Pemasiri, M. Montazeri, R. Gass, L. M. Smith, H. E. Jackson, J. Yarrison-Rice, S. Paiman, Q. Gao, H. H. Tan, C. Jagadish, X. Zhang, and J. Zou, Nano Lett. **9**, 648 (2009).
[11] M. Law, L. E. Greene, J. C. Johnson, R. Saykally, and P. D. Yang, Nat. Mater. **4**, 455 (2005).
[12] K. Q. Peng, Y. Xu, Y. Wu, Y. J. Yan, S. T. Lee, and J. Zhu, Small **1**, 1062 (2005).
[13] Y. Cui, Q. Q. Wei, H. K. Park, and C. M. Lieber, Science **293**, 1289 (2001).
[14] A. Kolmakov, Y. X. Zhang, G. S. Cheng, and M. Moskovits, Adv. Mater. (Weinheim, Ger.) **15**, 997 (2003).
[15] Y. Cui and C. M. Lieber, Science **291**, 851 (2001).
[16] X. F. Duan, Y. Huang, Y. Cui, J. F. Wang, and C. M. Lieber, Nature (London) **409**, 66 (2001).
[17] Y. Cui, Z. H. Zhong, D. L. Wang, W. U. Wang, and C. M. Lieber, Nano Lett. **3**, 149 (2003).
[18] X. F. Duan, C. M. Niu, V. Sahi, J. Chen, J. W. Parce, S. Empedocles, and J. L. Goldman, Nature (London) **425**, 274 (2003).
[19] M. H. Huang, S. Mao, H. Feick, H. Q. Yan, Y. Y. Wu, H. Kind, E. Weber, R. Russo, and P. D. Yang, Science **292**, 1897 (2001).
[20] P. D. Yang, H. Q. Yan, S. Mao, R. Russo, J. Johnson, R. Saykally, N. Morris, J. Pham, R. R. He, and H. J. Choi, Adv. Funct. Mater. **12**, 323 (2002).
[21] D. H. Zhang, Z. Q. Liu, C. Li, T. Tang, X. L. Liu, S. Han, B. Lei, and C. W. Zhou, Nano Lett. **4**, 1919 (2004).
[22] C. Borchers, S. Muller, D. Stichtenoth, D. Schwen, and C. Ronning, J. Phys. Chem. B **110**, 1656 (2006).
[23] P. Buffat and J. P. Borel, Phys. Rev. A **13**, 2287 (1976).
[24] S. J. Henley, J. D. Carey, and S. R. P. Silva, Phys. Rev. B **72**, 195408 (2005).
[25] P. Wynblatt and N. A. Gjostein, Prog. Solid State Chem. **9**, 21 (1976).
[26] B. K. Chakraverty, J. Phys. Chem. Solids **28**, 2401 (1967).
[27] S. A. Morin, M. J. Bierman, J. Tong, and S. Jin, Science **328**, 476 (2010).
[28] S. T. Ho, C. Y. Wang, H. L. Liu, and H. N. Lin, Chem. Phys. Lett. **463**, 141 (2008).
[29] C. Y. Geng, Y. Jiang, Y. Yao, X. M. Meng, J. A. Zapien, C. S. Lee, Y. Lifshitz, and S. T. Lee, Adv. Funct. Mater. **14**, 589 (2004).
[30] X. D. Wang, J. H. Song, C. J. Summers, J. H. Ryou, P. Li, R. D. Dupuis, and Z. L. Wang, J. Phys. Chem. B **110**, 7720 (2006).
[31] J. T. Hu, T. W. Odom, and C. M. Lieber, Acc. Chem. Res. **32**, 435 (1999).
[32] J. S. Jie, G. Z. Wang, X. H. Han, J. P. Fang, Q. X. Yu, Y. Liao, B. Xu, Q. T. Wang, and J. G. Hou, J. Phys. Chem. B **108**, 8249 (2004).
[33] I. Beszeda, E. G. Gontier-Moya, and A. W. Imre, Appl. Phys. A **81**, 673 (2005).
[34] H. Okamoto and T. B. Massalski, in *Binary Alloy Phase Diagrams*, edited by T. B. Massalski, H. Okamoto, P. R. Subramanian, and L. Kacprzak (ASM International, Materials Park, OH, 1990).
[35] X. J. Wang, G. P. Li, T. Chen, M. X. Yang, Z. Zhang, T. Wu, and H. Y. Chen, Nano Lett. **8**, 2643 (2008).
[36] N. Felidj, G. Levi, J. Pantigny, and J. Aubard, New J. Chem. **22**, 725 (1998).
[37] P. Ding and A. W. Pacek, J. Dispersion Sci. Technol. **29**, 593 (2008).
[38] W. C. Wang, D. Y. Zhong, J. Zhu, F. Kalischewski, R. F. Dou, K. Wedeking, Y. Wang, A. Heuer, H. Fuchs, G. Erker, and L. F. Chi, Phys. Rev. Lett. **98**, 225504 (2007).
[39] L. Huang, S. J. Chey, and J. H. Weaver, Phys. Rev. Lett. **80**, 4095 (1998).
[40] V. N. Antonov, J. S. Palmer, A. S. Bhatti, and J. H. Weaver, Phys. Rev. B **68**, 205418 (2003).